Vertical Structure of Ocean Surface Currents Under High Winds from Massive Arrays of Drifters

John Lodise[1], Tamay Özgökmen[1], Annalisa Griffa[2], Maristella Berta[2]

5 [1]RSMAS, University of Miami, Miami, FL, 33149, USA
[2]CNR-ISMAR, Lerici, Italy

Correspondence to: John Lodise (jlodise@rsmas.miami.edu)

Abstract. Very near surface ocean currents are dominated by wind and wave forcing and have large impacts on the transport of buoyant materials in the ocean, but have proved difficult to measure with many modern instrumentations. Here,
10 observations of ocean currents at two depths within the first meter of the surface are made utilizing trajectory data from both drogued and undrogued CARTHE drifters, which have draft depths of 60 cm and 5 cm, respectively. Trajectory data of dense, co-located drogued and undrogued drifters, were collected during the LAgrangian Submesoscale ExpeRiment (LASER) that took place from January to March of 2016 in the Northern Gulf of Mexico. Examination of the drifter velocities reveals that the surface currents become strongly wind- and wave-driven during periods of high wind, with the
15 pre-existing regional circulation having a smaller, but non-negligible, influence on the total surface velocity. During these high wind events, we deconstruct the full surface current velocities captured by each drifter type into their wind- and wave-driven components after subtracting an estimate for the regional circulation which pre-exists each wind event. In order to capture the regional circulation in the absence of strong wind and wave forcing, a Lagrangian variational method is used to create hourly velocity fields for both drifter types separately, during the hours preceding each high wind event. Synoptic
20 wind and wave output data from the Unified Wave INterface-Coupled Model (UWIN-CM), a fully coupled atmosphere, wave and ocean circulation model, are used for analysis. The wind-driven component of the surface current exhibits a rotation to the right with depth between the two surface layers measured. We find that the averaged wind-driven surface current from 0-5 cm (0-60 cm) travels at ~3.4-6.0 % (~2.3-4.1 %) of the wind speed, and is deflected ~5°-55° (~30-85°) to the right of the wind, reaching higher deflection angles at higher wind speeds. Results provide new insight to the vertical
25 shear present in wind-driven surface currents under high winds, which have vital implications for any surface transport problem.

Introduction

We use drogued and undrogued CARHTE drifters, having draft depths of 60 cm and 5 cm, respectively (Novelli et al., 2017), in order to measure the average very near surface currents in the Northern Gulf of Mexico. The data used for
30 analysis were collected during the LAgrangian Submesoscale ExpeRiment (LASER), a campaign in which over 1000 biodegradable CARTHE drifters were deployed during the winter of 2016 (Haza et al., 2018). Utilizing a subset of the

CARTHE drifters from the experiment, we focus on three synoptic scale, high wind events during which, wind and waves seem to dominate the forcing of the surface flows measured by both drifter types. The velocities of both drifter types are calculated along the drifter trajectories during periods of increasing winds. During these high wind events, we deconstruct the full surface current velocities captured by each drifter type into their wind- and wave-driven components after subtracting

5   an estimate for the regional circulation which pre-exists each wind event. We then report on the vertical shear of the wind-driven component of the surface current between the two surface layers measured.

        Very near surface currents are especially sensitive to wind and wave forcing, which dominate the dynamics in the upper few centimeters of the ocean (Wu, 1983). Plastics at the surface have been observed to be transported to our coasts by wind- and wave-induced currents and can be transported differentially depending on their buoyancy, which dictates their

10   positioning in the upper water column (Isobe et al., 2014). Through numerical modeling, Le Hénaff et al. (2012) found that wind- and wave-induced currents had a strong impact on the fate of surface oil during the Deepwater Horizon oil spill in 2010. Another modeling study showed that in extreme events like hurricanes, Stokes drift, or the forward velocity induced by the depth decaying orbital motion of waves (Stokes, 1847), plays a major role in accurately predicting the movement of Lagrangian particles at the surface (Curcic et al., 2016). Despite the drastic impact on the dispersal of buoyant pollutants,

15   wind- and wave-driven dynamics in the upper few centimeters are poorly understood and not resolved in modern operational ocean models, which have used a wide range of parameterizations of wind-driven dynamics over relatively deep surface layers, forced with climatological winds (Chassignet et al., 2003; Chassignet et al., 2007).

        Observational data that captures the vertical shear within the first meter of wind-driven surface currents is very limited in the real ocean as well. This is mainly due to the limitations of the instrumentation used to gather this physical data.

20   The majority of Lagrangian drifter studies have used classic drifter designs (e.g. CODE (Davis, 1985) and SVP drifters (Lumpkin and Pazos, 2007)) that span depths ranging from 1–30 m (Lumpkin et al., 2017), and are therefore unrepresentative of the wind forced current at the very surface. Acoustic Doppler Current Profilers (ADCP's) are not able to accurately measure velocities near an undulating boundary, making it difficult to sample surface layers above depths of 0.5 m (Cole and Symonds, 2015; Sentchev et al., 2017). High Frequency (HF) radars are known to measure vertically integrated

25   surface currents, with about 80 % of the radar signal originating in the upper 1 m, depending on the electromagnetic wavelength of the radar, such that vertical shear within this depth is not detectible in the measurement (Stewart and Joy, 1974; Röhrs et al., 2015). Using a novelty suite of instruments in the Gulf of Mexico, Laxague et al. (2017) observed wind- and wave-induced surface currents within 1 cm of the surface, under lower winds (U10 = 4 m s^{-1}), to be twice as fast as the average current over the first 1m and four times as fast as the average current over the upper 10 m, revealing the need for

30   increased vertical resolution of these measurements.

        Classical Ekman theory states that wind-driven currents at the very surface travel at a deflection angle of 45° to the right of the wind in the northern hemisphere, when one assumes a balance between Coriolis and friction under stationary, homogeneous conditions (Ekman, 1905). Laboratory studies have shown that total surface drift currents induced by wind and waves combined, travel at ~ 3.1 % of the wind velocity, with the wind-induced drift decreasing and the wave-induced drift

increasing, with increasing fetch (Wu, 1983). Various observational studies on wind-driven currents over the upper ~1 m of the surface, which utilized a range of different instruments including CODE or undrogued SVP drifters, HF radars, or ADCPs, have reported a wide range of deflection angles ranging from 15° to 90° to the right of the wind at varying wind speeds (Ardhuin et al., 2009; Poulain et al., 2009; Kim et al., 2010; Sentchev et al., 2017; Berta et al., 2018). Individual

5   results and details of these studies are presented in Table 1. These observational studies also report wind-induced currents alone to be anywhere from 0.4 % to 5 % of the wind velocity, over the upper ~1 m, showing that results may vary significantly based on environmental conditions and methodology (Ardhuin et al., 2009; Poulain et al., 2009; Kim et al., 2010; Sentchev et al., 2017; Berta et al., 2018).

Using drogued and undrogued CARTHE drifters, we are able to fill in part of this observational gap by observing

10   the vertical shear between the 0-5 cm and 0-60 cm layers of surface currents, during high wind conditions (~12-20 m s^{-1}). Additionally, we deconstruct the measured velocities in both surface layers to arrive at an estimate for the purely wind-driven current over the two surface depths. Upon inspection of the total velocity of the drifters during the high wind events, we hypothesize that there are three dominant components that drive the surface currents being measured: A wind-driven component, a wave-driven component, and the regional circulation that pre-existed each high wind event. Assuming a

15   simple linear superposition of the velocity components, we define the total depth averaged velocity captured by each drifter type as the integral:

$$\bar{u}_T = \int_0^h [\, u_s(z) + u_w(z) + u_{rc}(z) \,]dz, \tag{1}$$

where u_w is the purely wind-driven velocity, u_s is the Stokes drift velocity, u_{rc} is the regional circulation that exists before the increase in synoptic winds, z is the depth being evaluated and h is the draft depth of the respective drifter. Given this

20   definition of the total surface current, we neglect possible nonlinear interactions between velocity components, which will be considered in future investigations.

The three components in Eq. (1) were estimated as followed: u_s was calculated numerically with the Unified Wave INterface-Coupled Model (UWIN-CM, Chen et al., 2013) during the LASER campaign and stored for later analysis, u_{rc} is estimated from the dense population of drifters in the region in the hours preceding substantial increases in synoptic winds

25   using the LAgrangian Variational Analysis (LAVA, Taillandier et al., 2006) to create Eulerian velocity fields of the regional circulation, and we solve for u_w by subtracting the estimated regional circulation and Stokes drift velocity from the total depth averaged velocity measured by the drifters.

In the Northwestern Mediterranean Sea, the underlying geostrophic currents were shown to retain their structure and influence the surface flow under high wind forcing for time periods on the order of 2-3 days (Berta et al., 2018). In the

30   present study, the timescales over which the flow features of the regional circulation, u_{rc}, retain their structure under strong winds is difficult to determine given the current dataset. However, the subtraction of the pre-existing regional circulation from the total velocity of the drifters during the high wind events, shows a-posteriori, that the pre-existing regional

circulation retains its structure, to a reasonable extent, during the high wind analysis periods on which we focus. After subtracting the pre-existing regional circulation and numerically calculated Stokes drift velocity, u_s, from the full velocity, $\bar{u}_T$, of the drifters during each period of high wind, we are left with an estimate for the average, purely wind-driven current, u_w, over the two surface depths measured by each drifter type.

5   The paper is organized as follows: Section 2 describes the CARTHE drifters and the configuration of the Unified Wave INterface-Coupled Model. Section 3 explains the LAgrangian Variational Analysis (LAVA) used to create the estimated Eulerian velocity fields of the pre-existing regional circulation, as well as the calculations involved in the deconstruction of the total surface current, $\bar{u}_T$, along each drifter trajectory during the high wind events. Results are presented in section 4, with a discussion of the results following in section 5. Concluding remarks are presented in section 6.

10   **2. Data**

2.1 CARTHE Drifter

        The CARTHE drifter is a biodegradable surface drifter that consists of a Spot Trace GPS unit by Global Star, a torus float which contains the GPS housing, two interlocking panels that form the drogue, and a flexible rubber tube that connects the drogue and float (Novelli et al., 2017). During the LASER experiment, over 1000 CARTHE drifters were deployed with
15   drogues, however, over the first 7 weeks of the experiment approximately 40 % of the drifters lost their drogues (Haza et al., 2018). Drogued and undrogued drifters have draft depths of 60 cm and 5 cm, respectively, and have been extensively analyzed with respect to their specific drift characteristics during laboratory experiments performed by Novelli et al. (2017). For this study, a subset of co-located drogued and undrogued drifters from the LASER campaign are used for analysis, due to their opportunistic location during the passage of large atmospheric fronts across the Northern Gulf of Mexico.

20   Drogue loss during the experiment mostly coincided with large storm and wave events and the precision of the determined time of drogue loss was 0.5 to 3 hours for 85 % of the drifters (Haza et al., 2018). The method for drogue loss detection is based on the differential velocities of the drifters, as the undrogued drifters are preferentially accelerated by the higher velocities of wind- and wave-driven currents present in the shallower surface layer in which the undrogued drifters reside. In addition, undrogued drifters display a decreased, more sporadic GPS transmission rate, due to their tendency to be
25   flipped by large or breaking waves, which points the GPS antennae downwards, and reduces the ability of the GPS to transmit until the drifter is flipped upright again. Despite this, 80 % of the time intervals between transmissions by undrogued drifters are still between 4.5 and 5.5 minutes, but with notably higher outliers than the drogued drifters (Haza et al., 2018). The algorithm for drogue detection used by Haza et al. (2018) was validated using a subset of 50 drifters with known drogue status and was shown to distinguish drogued and undrogued drifters with an accuracy of 94-100 %. This very
30   successful drogue detection algorithm has provided the opportunity to utilize both drogued and undrogued drifters to study the variation of very near surface currents with depth (Haza et al., 2018).

GPS transmissions reported each drifter's location every 5 minutes during the experiment, with an accuracy of about 7 m. In addition to the extensive categorization of drogued and undrogued drifters, the drifter trajectory data were also quality controlled for missing transmissions and linearly interpolated to regular 15-minute intervals (Haza et al., 2018). Velocities were then calculated, resulting in estimates for the average velocity of each drifter over 15-minute intervals.

5   When using drifters to study ocean currents, concerns about different sources of velocity slip must be addressed. Extensive laboratory testing performed by Novelli et al. (2017) using half-scale drogued and undrogued drifters showed that in the absence of wind and waves drogued (undrogued) drifters travel within 0.01 m s^{-1} (0.02 m s^{-1}) of the mean Eulerian current averaged over the draft depth of the given drifter. Under the effects of waves the undrogued drifter unsurprisingly feels an acceleration due to stokes drift, but the drogued drifter feels a reduced wave-induced acceleration due to the flexible
10   tether holding together its float and drogue. This mechanical decoupling partially removes the effect of the Stokes drift acting on the drogued drifter, mainly dampening the effects of stokes drift above the drogue (Novelli et al., 2017).

To characterize the slip velocity associated with wind, waves, and Eulerian current, Novelli et al. (2017) defines the "absolute" slip velocity as the difference between the velocity of a drifter and the depth integrated current over each drifters' draft. The absolute slip velocity of both drogued and undrogued drifters during laboratory testing was found to decrease with
15   increasing wind speed, decreasing from 3 cm s^{-1} to 0.1 cm s^{-1} for the drogued drifter and from 14 cm s^{-1} to 1 cm s^{-1} for the undrogued drifter, for wind speeds from 8.1 m s^{-1}to 23 m s^{-1}. This phenomenon is thought to be caused by wind separation from the ocean surface due to the presence of surface gravity waves (Novelli et al., 2017). Another laboratory experiment, focused on measuring the turbulent air flow over wind generated waves in a similar wind-wave tank, found wind separation to occur over 90 % of short wind waves at 10 m wind speeds of ~16 m s^{-1} (Buckley and Veron, 2017). The extent to which
20   wind separation occurs and its effectiveness of sheltering the drifters from wind-slip in the real ocean is difficult to quantify given the scale differences between the laboratory wave tank and open ocean. However, another recent experiment using full size CARTHE drogued and undrogued drifters in the real ocean, alongside a suite of instruments including an ADCP and polarimetric camera, showed that velocities calculated using both drifter types fell within the range of velocities measured by other instrumentation over the corresponding draft of each drifter (Laxague et al., 2017).

25   **2.2 UWIN-CM**

During the extent of the LASER campaign, daily 72 hour real-time forecasts were produced using the Unified Wave Interface-Coupled Model (UWIN-CM), running a fully-coupled atmosphere, surface gravity wave, and ocean circulation system (Chen et al., 2013; Chen and Curcic, 2016). The UWIN-CM model atmospheric component is comprised of the atmospheric non-hydrostatic Weather Research and Forecasting (WRF) model featuring Advanced Research WRF
30   dynamical core with 4 km horizontal resolution over the Gulf of Mexico with 36 vertical layers (Skamarock et al., 2008; Haza et al., 2018).

The surface gravity wave model is the University of Miami Wave Model v2 (UMWM, Donelan et al., 2012), with the same 4 km resolution as the atmospheric component. The three-dimensional Stokes drift velocity fields are calculated as the full integral:

$$u_S = \int\limits_{0}^{2\pi} \int\limits_{0}^{\infty} \omega k^2 \frac{cosh[2k(d+z)]}{2 sinh^2 kd} F(k, \theta) dk d\theta, \tag{2}$$

5   where ω is the angular frequency, k is the wavenumber, d is the mean water depth, z is the depth being evaluated, F is the wavenumber energy spectrum, and θ is the direction of the waves (Stokes, 1847; Phillips, 1977). The Hybrid Coordinate Ocean Model (HYCOM) v2.2 is used as the ocean circulation model, however no model output from this circulation model is used for the analysis of wind-driven currents. The surface layer of the HYCOM model has a minimum thickness of 3 m, which makes the model unrepresentative of the depths sampled by the drifters and very difficult to validate with

10   observational data (Wallcraft et al., 2009).

     The UWIN-CM model is initialized daily using initial and boundary conditions from Global Forecast System (GFS) and global HYCOM fields along with the previous day's UMWM wave forecast. Coupling between models is executed using the Earth System Modeling Framework (ESMF) in which all components are exchanged between models every minute (Hill et al. 2004). Hourly 10 m wind (U10) and Stokes drift velocity data from the 24th – 48th hour of each daily

15   72 hour forecast were stored and used for the analysis performed in this study. Initially having a temporal resolution of 1 hour, the UWIN-CM model output was interpolated to 15-minute intervals to match the time resolution of the drifter data.

3 Methods

3.1 High Wind Events and Region of Interest

     The domain for this study lies to the east and southeast of the Mississippi River Delta spanning from 27.5°N to 30.5°N

20   and 90°W to 86.5°W. The spatial extent of the data used for each high wind event are outlined in Fig. 1, along with NDBC buoy locations used for verification of the UWIN-CM wind data. Initial deployment of these drifters occurred during January and February of 2016 with the intent of capturing submesoscale dynamics on spatial scales of tens of meters to tens of kilometers (Haza et al., 2018). The large number of drifters deployed during the LASER campaign, and their relatively long transmission period of about 3 months, provided opportunity to collect data over a range of scales and environmental

25   conditions. The region and time periods chosen exhibit large numbers of co-located drogued and undrogued drifters during the passage of synoptic atmospheric fronts, which drive a large momentum input into the oceanic boundary layer.

     For this study, we choose to focus on three high wind events that occurred on January 22nd, February 24th and March 20th of 2016. Available wind data from nearby NDBC buoys (BURL, 42040 and 42012), along with the UWIN-CM wind data associated with each drifter position during and before the high wind event are plotted in Fig. 2. The time periods

30   over which we perform the deconstruction of the total measured surface currents during each high wind event are marked by vertical black lines, and the red solid and dashed vertical lines show the start of the hour over which the pre-existing regional

circulation is estimated from drogued and undrogued drifters, respectively (Fig 2). Validation of the UWIN-CM U10 output with available NDBC buoy data revealed that during the passage of atmospheric fronts through the domain there exists a fair amount of variability in the modeled wind magnitude resulting, at times, in a large difference between observed and modeled data. For this reason, we exclude any data associated with modeled wind magnitude ranges above 6 m s^{-1} at any given 15-minute time step.

3.2 LAgrangian Variational Analysis (LAVA) and Pre-existing Regional Circulation

Initial inspection of the total drifter velocities during each high wind event showed larger than expected spatial variation in drifter velocities, including velocities which depict surface currents traveling to the left of the wind, which challenges previous wind-driven surface current theory and observations. Previous works that have studied instantaneous wind-driven dynamics over a range of spatial scales have illustrated the need to account for the circulation present before the observed increase in synoptic winds in order to isolate the wind-driven component of the flow (Sentchev et al., 2017; Berta et al., 2018). Based on these studies, we hypothesize that the spatial variability observed in the total velocities is due to the regional circulation that pre-existed the period of increasing winds, which retains its structure on times scales long enough to influence the surface flow during each high wind event.

In order to resolve surface currents in our region of interest at adequate spatial and temporal resolution we utilize the Lagrangian Variational Analysis (LAVA, Taillandier et al., 2006) and the available drifter data in the region to estimate the regional circulation. Geostrophic velocities derived from altimetry data and surface Ekman current velocities parameterized using forecasted winds have been shown to have inadequate spatial and temporal resolution, in order to accurately estimate surface currents in the Northern Gulf of Mexico on scales less than the order of 100 km in space and 1 week in time (Berta et al., 2015). LAVA allows us to use the undrogued and drogued drifter trajectory data in the region, to create Eulerian velocity fields that are statistically robust and on the spatial and temporal scales on the order of 10 km and hours, respectively (Taillandier et al., 2006; Berta et al., 2015). LAVA has been used in previous studies to create velocity fields using purely Lagrangian data, as well as blending drifter trajectory data with Eulerian velocity fields derived from altimetry and HF radars. LAVA has proven especially useful when providing Near Real Time (NRT) information that can be useful to first responders of oil spills, search and rescue efforts and other surface transport problems (Taillandier et al., 2006; Chang et al., 2011; Berta et al., 2014; Berta et al., 2015).

Given our hypothesis that during the high wind events, the total velocity of the drifters is partly composed of the regional circulation that pre-existed the onset of high winds, an estimate for this circulation must be removed from the total velocity of the drifters in order to isolate the wind- and wave-driven components. We utilize LAVA and the available drogued and undrogued drifter data in the region to create semi-simultaneous hourly Eulerian velocity fields for both drifter types, separately. The drifters used for the velocity field construction for each event are plotted in Fig. 3. The January 22nd event occurred very close to the initial time of deployment while the drogued drifters were still tightly packed spatially and little drogue loss has occurred, leaving a smaller, but adequate, number of undrogued drifters to utilize for the estimate of the

pre-existing circulation. The events on February 24th and March 20th, occur long enough after deployment, thus resulting in a more even amount of drogued and undrogued drifters that are also more evenly spread through the region, however drogued drifters do show a tendency to converge upon one another, evident in the spatial organization of the drifters seen in Fig. 3.

LAVA utilizes drifter trajectories in order to create average velocity fields over multiple time steps depending on the

5   parameters R, T_a, Δt and Δx, which need to be prescribed before implementation of the analysis. R determines the spatial range over which the velocity of each drifter is spread from the drifter location through finite iterations of the diffusion equation and should be chosen as the typical length scale, or Rossby radius, for the targeted oceanic dynamics to be resolved in the given region. For this analysis, R is set to 10 km, which is same value used for a previous study which utilized drifter data in the same region of the Northern Gulf of Mexico (Berta et al., 2015). Δt for this study is 15 minutes, which is the time

10   resolution of the quality controlled drifter trajectories which have been linearly interpolated to regular 15-minute intervals (Haza et al., 2018). The analysis time scale, T_a is the larger time window over which consecutive velocity fields created using LAVA are averaged and should be shorter than the Lagrangian time scale (Taillandier et al., 2006). Lagrangian time scales within this region have been calculated to be as small as ~1-3 hours, which corresponded to spatial scales ranging from .4-3.5 km (Gonçalves et al., 2019), and as large as ~1-3 days corresponding to spatial scales ranging from ~10-35 km

15   (Ohlmann and Niiler, 2005). Here, T_a is set to 1 hour, which is adequately short given our assignment of 10 km as the typical horizontal length scale being resolved by LAVA. Δx is the spatial resolution of the discretized velocity field and needs to be assigned such that Δx < R, defined here as Δx = 1.5 km. (Taillandier et al., 2006; Berta et al., 2015). Drifter trajectories within $2\Delta x$ of one another are averaged to become single drifter trajectories positioned along their center of mass before the production of Eulerian velocity fields (Berta et al., 2015).

20   After the Eulerian velocity fields are created, a kinetic energy mask is also implemented to exclude small velocities that are an artifact of assigning radially decreasing velocities away from drifter locations using LAVA. To avoid these unrealistically small velocities, any values in the Eulerian velocity fields that represent less than 10 % of the hourly averaged kinetic energy in the velocity field are discarded. This relatively low threshold of kinetic energy was chosen to maximize the coverage between the Eulerian velocity field estimates of the pre-existing regional circulation and drifter trajectory data

25   during each high wind event.

The hourly velocity fields are created during low wind conditions, hours before the passage of synoptic scale atmospheric fronts, which produce very high winds over the entire region. To avoid unnecessarily smoothing the Eulerian velocity fields through averaging, we choose one hourly velocity field per event, per drifter type, to use for analysis. Hourly Eulerian velocity fields are chosen based on the criteria that there are relatively low wind velocities present, the time gap

30   between the velocity field and onset of high wind isn't needlessly long and how well the Eulerian velocity field overlies the drifter trajectories during the high wind event. The Eulerian velocity fields used for analysis are plotted in Fig. 4 and labelled with the beginning of the hour over which they were created. The hour over which these velocity fields are created are also indicated in Fig. 2.

3.3 Deconstruction of Total Surface Current

The total surface current, $\bar{u}_T$, calculated between each 15-minute drifter position during the high wind event, is stored at the later drifter coordinate used for each calculation. The beginning of the analysis during the high wind period, is such that a widespread velocity change due to the wind is observed in the drifter trajectories and the drifters enter the region

5   where an observation of the pre-existing regional circulation exists. In addition, we stop the analysis for each high wind event at the apex of the increasing wind velocity magnitude, beyond which the drifters exhibit large inertial motions due to the decrease in momentum input from the wind. The drifter trajectories, during the period over which the deconstruction of the total surface current are made, are shown in Fig. 5.

From the full drifter velocities, calculated on 15-minute intervals during each wind event, we subtract the nearest

10   point velocity in the estimated Eulerian velocity field of the pre-existing regional circulation, u_{rc}. Each Eulerian velocity field has a spatial resolution of 1.5 km, which is adequate to preserve the flow features given the typical length scale of 10 km in the region (Berta et al., 2015). In the event that the nearest point to the drifter location in the regional circulation velocity estimate does not have a value, due to lack data in the velocity field created before the increase in synoptic winds, the data is discarded. The trajectories in Fig. 5 are color coded to show where the drifter trajectories and Eulerian velocity

15   fields overlap during the high wind event and where data coverage is missing.

The subtraction of multiple hourly adjacent velocity fields, earlier and later in time, were examined a-posteriori for each event and found to produce similar end results. The hourly Eulerian velocity fields chosen for this analysis were those that had the most data points in common with the respective drifter trajectories during the high wind event, or those that retained a similar amount of data points during the subtraction (within 3.5 % of the maximum amount of retained trajectory

20   data for each specific case) but resulted in larger decreases in the standard deviation of the deflection angle between drifters and wind velocity. This decision is motivated by the assumption that the isolated effects of wind and waves will result in a more directionally uniform velocity field, than that of a surface flow being influenced by the regional circulation estimates shown in Fig. 4. Thus, by removing more variation in the deflection angles between the wind and drifter velocities, we better represent the combined wind- and wave-driven components, assuming the wind and wave directions are well aligned. All

25   velocity estimates and calculations are performed using drogued and undrogued drifter data, separately.

After subtracting the pre-existing regional circulation from the full drifter velocities during the high wind events, the remaining velocity is an estimate for the combined wind- and wave-driven flow ($u_s + u_w$), referred to here after as the wind-wave-driven velocity. To further deconstruct this velocity estimate, we subtract the UWIN-CM modeled Stokes drift velocity (u_s) fields, again at the nearest point to each drifter location for each 15-minute interval. Because the large wind-

30   driven events being analyzed are of synoptic scale, the UWIN-CM modeled Stokes velocity and U10 winds are relatively uniform in the region of study, making the 4 km resolution of the data adequate to perform meaningful calculations in this manner.

Because the drogued drifters display a filtering characteristic of the surface Stokes drift, as illustrated in laboratory testing performed by Novelli et al. (2017), the stokes drift at 0.4 m depth is used for the calculation with drogued drifter-derived velocities (0.4 m being the vertical center of the drogue). From the undrogued drifter associated velocities, we subtract the surface ($z = 0$ m) Stokes drift velocity. After subtracting the wave-driven component, u_s, from the wind-wave-

5   driven velocity, we are left with an estimate for the average wind-driven velocities, u_w, over each respective drifter draft depth. The average wind-wave-driven and wind-driven velocities are compared to the modeled U10 wind data, using the U10 wind velocity datum at the nearest point in the modeled Eulerian field to each drifter location at every time step.

4. Results

Figure 4 shows the estimated Eurlerian velocity fields of the regional circulation that pre-existed each given high

10   wind event, for each drifter type. The main flow features seen in the estimated Eulerian velocity fields show evidence of flow features having spatial scales on the order of tens of kilometers. Observations of smaller flow features are limited by the 1.5 km resolution and typical length scale of 10 km set by the chosen LAVA configuration. The regional circulation observed, by either drifter type, prior to the wind events on February 24th and March 20th show an abundance of meanders, eddies and frontal features, whereas the regional circulation pre-existing the wind event on January 22nd suggests that a

15   somewhat larger feature, closer to the order of 100 kilometers, is driving the majority of the flow to the northeast with some variability seen throughout the flow. Features on these spatial scales (10-100 km) are known to have characteristic time scales on the order of days to weeks (Özgökmen et al., 2016) which suggests that the main flow features observed in the pre-existing regional circulation, are likely retain their overall structure, to a certain extent, during of the high wind analysis periods presented here.

20   The trajectories of both drogued and undrogued drifters during the hours of increasing winds, over which the total velocity deconstructions were performed are shown in Fig. 5. Overall the trajectories show that the larger scale, synoptic winds and coinciding wave-induced motions are the dominant driving force in the drifter movement, evident in the similarities in drifter tracts across each domain. Influence of the pre-existing regional circulation can also be observed, evident in the variability among drifter trajectories. The undrogued trajectories seem to show less variability across the

25   domain than for the drogued case, suggesting the wind- and wave-driven components are even more dominant in the surface layer measured by the undrogued drifters.

Scatter plots of the difference between the wind direction and the direction of the total velocity of the drogued and undrogued drifters, i.e. deflection angles, along the trajectories segments shown in black in Fig. 5, are shown in Figs. 6a and 6b, respectively. Figures 6c and 6d show the deflection angles between the wind and drifter velocities, after the Eulerian

30   velocity field estimates of the pre-existing regional circulation (Fig. 4) have been subtracted from the full velocity of the drifters. Any data points lost during the subtraction of the regional circulation velocity field, shown as red segments in Fig. 5, were also excluded from the scatter plots showing the full drifter velocities (Fig. 6a, b) for accurate comparison. Deflection angles are plotted against the point value wind magnitude from the UWIN-CM model, closest to the drifter location at the

time of the velocity measurement. It is evident from Fig. 6 that the scatter of the total drifter velocity deflection angles has a wider, more disorganized spread than the deflection angles calculated after the pre-existing regional circulation has been removed from the full velocity. This is especially apparent for the drogued drifter case.

5   The average velocity magnitude of the calculated wind-wave-driven currents is compared to the average magnitude of the pre-existing regional circulation for each wind event and drifter type in Fig. 7. The magnitude of the regional circulation is plotted as a percentage of the combined wind- and wave-driven velocity magnitude. This percentage decreases as the wind- and wave-driven effects become increasingly large during each high wind event. During the analysis periods over which we deconstruct the total surface current (shown by vertical lines in Fig. 7), the pre-existing circulation is 30-45 % as large as the combined wind-wave-driven velocity calculated using drogued drifters, and 25-30 % as large as that measured

10 by undrogued drifters.

      The wind-wave-driven, wind-driven, and wave-driven (Stokes drift) velocities are binned by wind magnitude on 0.5 m s^{-1} intervals. The total number of drifter positons, per wind bin, where the surface velocity deconstruction is performed, are plotted in Fig. 8, which shows that the most robust results exist over wind bins from 14.5-18 m s^{-1} for both drogued and undrogued drifters. It should be noted that although the sample size varies considerably between drifter types and over the

15 assigned wind bins, both drifter types have substantial sample sizes over most wind bins presented, given the relatively short time periods of analysis. The sample size of drifter measurements is also listed for each high wind event in Fig. 5. Averages and standard deviations of the velocity components were computed within each bin. The average deflection angle from the wind direction of the Stokes velocity, wave-wind-driven velocity and wind-driven velocity for each respective drifter draft depth are shown in Fig. 9. The magnitudes of the same velocity components are plotted as a percentage of the wind

20 magnitude in Fig. 10. Figures 9c and 10c are obtained by subtracting the given Stokes drift velocity (Figs. 9a, 10a) from the estimated wind-wave-driven velocities (Figs. 9b, 10b). Bins lower than 11.5 m s^{-1} have been omitted in Figs. 9 and 10, due to lack of data points and large variation of deflection angle in the given bins. Error bars indicate one standard deviation about the mean for each bin (Figs. 9 and 10).

5. Discussion

25   Comparison of scatter plots in Fig. 6 indicate that the pre-existing regional circulation still influences the surface currents over the depths measured by both drifter types during a large wind-driven event. The scatter of deflection angles between different drifter types also suggests that the relatively deeper layer measured by the drogued drifter exhibits larger variation in velocity due to the regional circulation component of the flow. The shallow layer, observed with undrogued drifters, seems to be more dominantly driven by the wind and wave components, as removing the influence of the regional

30 circulation results in a less drastic compression of the scatter. In both the drogued and undrogued cases, the removal of the estimated regional circulation results in a decrease in the standard deviation of the surface current deflection angle for all wind bins from 11.5-20 m s^{-1}.

Comparison of the combined wind-wave-driven currents and the pre-existing circulation estimates confirms that the surface velocities are dominantly wind- and wave-driven. Figure 7 shows that on average, during the high wind analysis windows (shown by vertical dashed lines), the pre-existing circulation is only ~25-30 % as strong as the combined wind-wave-driven flow measured by the undrogued drifters. Drogued drifter measurements during the same periods also show that

5   the pre-existing circulation is relatively weaker (~30-45 % of the combined wind-wave-driven velocity magnitude over the drogued drifter depth). Analysis of the plots in Fig. 7, led the authors a-posteriori, to determine the optimal windows for the velocity deconstruction results during the high wind events. With respect to the subtraction of the pre-existing regional circulation and the improvement of the scatter in deflection angles (seen Fig. 6), the most robust results, for both drifter types, occur when the relative strength of the wind-wave-driven flow to the pre-existing regional circulation reaches a

10   plateau (seen in Fig. 7). This is also when the wind, and therefore the wind-wave-driven component, is the strongest, which suggests that any error introduced during the velocity deconstruction makes up a smaller percentage of the calculated velocities. Extending the velocity deconstruction analysis windows, by 2 hours before and 2 hours after, does not significantly change the averages and trends shown in Figs. 9 and 10, but does however, slightly disorganize the scatter of the deflection angles seen in Fig. 6c,d. This investigation of sensitivity also aided in determining the optimal time periods for

15   analysis.

In the upper 5 cm, the average wind-wave-driven component of the flow varies with increasing wind speed, traveling between ~4° and 40°, to the right of the wind, as winds increase from 11.5-20 m s^{-1} (Fig. 9b). On average, the magnitude of this flow varies from 4.5-7.1 % of the wind speed (Fig. 10b). Over the deeper surface layer (0-60 cm), the deflection angle of the wind-wave-driven current varies from ~26°-60°, as winds increase over the same range, traveling at

20   2.8-4.6 % of the wind speed, on average (Figs. 9b and 10b). The total wind-wave-driven flow in both layers exhibit larger deflection angles as wind speeds increase, with the 0-60 cm layer travelling at a slower velocity, and being deflected ~5°-28° further to the right than the 0-5 cm layer. Since the deflection angle of the Stokes drift velocity (Fig. 9a) is almost constant with wind speed, the increase in deflection angle seen in Figs. 9b and 10b, is most likely due to a change in the wind-driven momentum input.

25   Classical Ekman theory is based on the balance between Coriolis and vertical viscosity in the water column, which given the parameterization for wind stress and viscosity assigned by Ekman (1905), results in a wind-driven surface current deflected 45° to the right of the wind in the Northern Hemisphere, which spirals to the right and decreases in magnitude with depth. In contrast to Ekman, the "Slab" solution, based on enhanced surface mixing due to breaking waves and shear-induced turbulence, prescribes a linear decrease of wind stress with depth, resulting in a surface current which travels 90° to

30   the right of the wind, uniformly with depth (Pollard and Millard, 1970). Both of these theories are formed under idealized situations, which under represent other ocean processes associated with wind-driven dynamics, possibly the most significant being Stokes drift. We can however, make a reasonable comparison to these theoretical results after the wind-driven component is isolated from the other components that make up the total drifter velocities.

Our estimates for purely wind-driven surface currents over the two layers measured (Figs. 9c and 10c) show the upper 5cm layer traveling ~5° to the right of the wind, at 6.0 % of the wind speed during 12 m s^{-1} winds. The deflection angle gradually increases to ~55° to the right of the wind as wind speeds increase to 20 m s^{-1}. The average velocity magnitude varies between 3.4-6.0 % of the wind speed over this wind interval. The deflection angle of the wind-driven

5   surface current residing in the upper 60 cm ranges from ~30°-85°, again with higher deflection angles occurring at higher wind speeds. The velocity magnitude of this wind-driven layer varies from 2.3-4.1 % of the wind speed over the given wind speed interval. The difference in deflection angle between layers varies between ~8° and 30°, with the deeper layer traveling further to the right, at a slower velocity. In both cases there seems to exist an increase in deflection to the right with increasing wind speed. These findings seem to support aspects of both the Ekman and Slab solutions, as there does appear to

10   be a rotation of the surface current with depth, however, both layers display a larger deflection than predicted by Ekman at larger wind speeds. This can possibly be explained by enhanced vertical mixing under high wind and wave conditions, which is thought to distribute wind-driven momentum into the water column. This theory motivates the assignment of a linearly decreasing wind stress with depth used in the slab model solution by Pollard (1970) which results in deflection angles of 90 degrees over all depths of the mixed layer. The observed increase in deflection angle with wind speed may suggest a gradual

15   change in wind-driven flow regimes, from surface Ekman dynamics to more Slab-like dynamics, as increasing wind velocity and subsequent turbulence from vertical shear and breaking waves, mix momentum vertically in the wind-driven layer. However, there still exists a rotation of the wind-driven current with depth which cannot be explained using slab-like dynamics alone.

Comparison to more recent observational studies is nontrivial due to differences in instrumentation, measurement

20   depth, and time resolution of measurements. Many previous studies have performed spectral analysis on years of HF radar or drifter data with time resolutions varying from 1-6 hours, and calculated correlations between wind and surface currents in order to isolate the wind-driven component of the flow. Results from these studies find a range of deflection angles from 17-90 degrees to the right of the wind, with current magnitudes varying from 0.4-5 % of the wind speed. (Ardhuin et al., 2009; Poulain et al., 2009; Kim et al., 2010). Sentchev et al. (2017) used instantaneous vertical ADCP measurements to calculate

25   the wind-driven effect on surface currents (0.5-75m depth) during sea breeze conditions (wind speeds of ~3-6 m s^{-1}), finding wind-driven deflection angles of 12°-25° and current magnitudes of 2-4 % of wind speed. The study also found a rotation to the right was present between wind-driven velocities of increasing measurement depth. Berta et al. (2018) used hourly HF radar measurements to observe the influence of large wind events lasting 1-3 days. After subtracting the geostrophic component of the flow to isolate the wind-driven current, they found surface velocity deflection angles and magnitudes of

30   25-30° and ~2 % of the wind speed, respectively. More details of these previous studies on wind-driven dynamics can be found in Table 1.

The findings portrayed in this paper seem to be within the range of previously reported results for wind-driven surface flows with discrepancies likely resulting from the differences in the depth of the measurement, range of wind

magnitudes, or methodology in isolating the wind-driven component. With the exception of Ardhuin et al. (2009), none of these studies account for Stokes drift in their measurements possibly resulting in smaller deflection angles due to the near alignment of winds and wave direction (Poulain et al., 2009; Kim et al., 2010; Sentchev et al., 2017; Berta et al., 2018). The UWIN-CM modeled Stokes velocity used for this study, seems to be in good agreement with the full Stokes velocity magnitude and deflection angle presented by the previous literature (Ardhuin et al., 2009).

5 One source of error in the wind-driven measurements reported here is the possible evolution of the regional circulation during the time gap between the observation of the pre-existing regional circulation and the velocity deconstruction during the high wind period. Although it is difficult to quantify given the available data, the regional circulation is evolving, to a certain extent, during the time gap between the observation of the regional circulation and the

10 analysis periods of high winds. In addition, the regional circulation could begin to be modified through interactions with the large wind- and wave-induced currents. The overall timescales on which these flow features evolve or are altered by each high wind event is beyond the scope of this paper, given the available data set. However, the relatively short time scales of these periods of high winds should limit the errors introduced by the evolution of the pre-existing circulation. The decreased variability seen in the deflection angles after the subtraction of the pre-existing regional circulation (Fig. 6) suggests, a-

15 posteriori, that the regional circulation does maintain its structure to a reasonable extent during the periods of increasing winds being analyzed.

Another possible source of error comes from the velocity slip characteristics of the drifters mentioned above, mostly relevant in the undrogued case. The magnitude of the wind-wave-driven and purely wind-driven velocities calculated using undrogued drifters are among the higher estimates previously reported (Ardhuin et al., 2009; Poulain et al., 2009; Kim et al.,

20 2010; Sentchev et al., 2017; Berta et al., 2018). The effect on the velocity slip of these drifters due to windage and wave steepening has been documented by Novelli et al. (2017). Although there exists a large difference in scales between the lab and the real ocean, the differences between the combined wind-wave-driven velocity magnitudes of drogued and undrogued drifters (~2 % of the wind speed on average) in the current study, are in good agreement to that of laboratory studies using half scale drifters and a past field experiment using full size drifters (Laxague et al., 2017; Novelli et al., 2017). As

25 mentioned above, laboratory testing of undrogued drifters showed that the total velocity slip could be as high as 14 cm s^{-1}, but was shown to decrease to only 1 cm s^{-1} with increasing wind speeds (over a range of 15-23 m s^{-1} in the lab) due to the sheltering of drifters from the wind by increasing wave heights (Novelli et al., 2017). This could partly explain the gradual decrease in wind-driven velocities for both drifter types from wind bins 11.5-18 m s^{-1}, especially given the relatively high wind-driven velocities seen at lower wind bins. Exactly how much wind-slip is occurring during specific wind velocities and

30 wave heights in the real ocean is difficult to determine, but the average magnitude of the observed vertical shear seems to be in relatively good agreement with past experiments and laboratory testing performed with these drifters (Laxague et al., 2017; Novelli et al., 2017).

The momentum input from large breaking waves into the surface currents at the very high wind speeds studied here, could also cause an increase in velocities observed in the wind-driven surface currents. Ardhuin et al. (2009) attributes larger deflection angles of wind-driven currents to enhanced mixing due to wave breaking, which could be a congruous theory to our observation of increasing deflection angles at higher wind speeds. Enhanced mixing caused by breaking waves, acts to

5   mix the vertical momentum of surface currents, likely resulting in larger deflection angles at shallower depths (Rascle et al., 2006).

The results presented here, to the authors' knowledge, are the first reported estimates of the vertical shear of wind- and wave-driven currents in the upper 1 meter of the ocean under this regime of high winds (11.5-20 m s^{-1}). The combined wind-wave-driven velocity in the upper 5 cm calculated here is, on average, ~1.6 times greater than that measured over 0-60

10   cm for the wind magnitudes presented. These results support the finding of Laxague et al. (2017), which showed that total surface currents in the upper 1 cm are twice as fast as the average current over the first 1 m due to wind- and wave-driven vertical velocity shear. The true novelty of the results presented here lies in the estimates for the vertical shear of the purely wind-driven surface current over the 0-5 cm and 0-60 cm layers. The deconstruction of the total velocity measured from drogued and undrogued drifters gives us an estimate of the wind-driven vertical shear directly at the ocean's surface, which

15   has proved difficult to measure by previous studies and has significant implications for surface transport problems in the real ocean.

The high wind events focused on here only occurred for a small number of days during the LASER campaign, which is typical for the Northern Gulf of Mexico in the winter. Since the velocity profile within upper meter has been shown to be very dynamic, being affected by the general oceanic circulation as well as local wind-wave-driven mechanisms, it is

20   important to observe near surface currents under different environmental conditions and at greater vertical resolution. Attention also needs to be given to the transport of Lagrangian particles by breaking waves which induce vertical motion and mixing which can alter wind-driven currents.

6. Conclusion

We use a combination of stored output data from the UWIN-CM fully coupled atmospheric-wave-ocean model and

25   observational trajectory data from both drogued and undrogued CARTHE drifters to calculate an estimate for purely wind-driven currents during periods of strong, increasing winds. The use of co-located drogued and undrogued drifters provides measurements for the vertical shear between the upper 5 cm and upper 60 cm surface layers. Using the LAgrangian Variation Analysis, we are able to create velocity fields in the hours leading up to the high wind events studied, that serve as an estimate for the pre-existing regional circulation which is found to still affect the surface velocities during periods of high

30   winds. After subtracting the regional circulation from our measured drifter velocities we analyze the relationship between wind velocity, Stokes drift, and wind-driven current over the draft depth of the drifters. On average, we find the wind-driven current to decrease in magnitude and rotate to the right of the wind with depth, with the upper 5 cm (60 cm) traveling ~5°-

55° (~30°-85°) at 3.4-6.0 % (2.3-4.1 %) of the wind speed over the range of 12-20 m s^{-1}. Both surface layers display an increase in deflection angle with increasing wind speed, sustaining an average difference of 8°-30° between flow directions.

   This study is among the few (Sentchev et al., 2017; Berta et al., 2018) that have investigated the real-time response of very near surface currents to increasing wind. We are able to observe characteristics of the vertical shear present between
5 the upper 60 cm and 5 cm of wind driven surface currents. Observations of vertical shear this close to the surface in the real ocean, especially during high wind events of this nature, are very scarce due to the limitations of present day instrumentation. The vertical velocity profile within the upper meter has been shown to exhibit a large amount of shear, with velocities at the surface (upper few centimeters) being largely dominated by wind and waves (Laxague et al., 2017). This highlights the importance of very near surface observations, such as those presented in this paper, as this vertical shear can
10 have large impacts on the transport of pollutants of varying size and buoyancy, like plastics and oil. Incorporating vertical shear due to wind and waves within the upper meter, could have important implications for fate prediction of pollutants transported at the ocean surface.

   Data Availability. Raw, processed drifter trajectory data, and drogue classification are publicly available through the Gulf
15 of Mexico Research Initiative Information & Data Cooperative (GRIIDC) at https://data.gulfresearchinitiative.org under https://doi.org/10.7266/N7MS3R6V,   https://doi.org/10.7266/N7W0940J,   and   https://doi.org/10.7266/N7QN656H, respectively. The UWIN-CM data can also be obtained from GRIIDC under https://doi.org/10.7266/N7KW5DH7.

   Competing interests. The authors declare that they have no conflict of interest.

20 **Author Contribution.** The formal analysis was carried out by JL as a PhD candidate under the supervision of TO. All authors contributed in the conceptualization of the work. MB educated JL on the necessary algorithm (LAVA) used to performed the formal analysis.

   Acknowledgements. This research was made possible by a grant from The Gulf of Mexico Research Initiative. The authors would like to thank all those involved in planning and executing LASER, as well as the scientists involved with the data
25 processing and drogued detection that made this analysis possible.

   References

Ardhuin, F., Marié, L., Rascle, N., Forget, P. and Roland, A.: Observation and estimation of Lagrangian, Stokes, and
   Eulerian currents induced by wind and waves at the sea surface, J. Phys. Oceanogr., 39, 2820-2838,
30   http://doi:10.1175/2009JPO4169.1, 2009.

Berta, M., Bellomo, L., Magaldi, M.G., Griffa, A., Molcard, A., Marmain, J., Borghini, M. and Taillandier, V.: Estimating
   Lagrangian transport blending drifters with HF radar data and models: results from the TOSCA experiment in the

Ligurian Current (North Western Mediterranean Sea). Prog. Oceanogr., 128, 15-29, https://doi.org/10.1016/j.pocean.2014.08.004, 2014.

Berta, M., Griffa, A., Magaldi, M.G., Özgökmen, T.M., Poje, A.C., Haza, A.C. and Olascoaga, M.J.: Improved surface velocity and trajectory estimates in the Gulf of Mexico from blended satellite altimetry and drifter data, J. Atmos. Ocean. Tech., 32, 1880-1901, https://doi.org/10.1175/JTECH-D-14-00226.1, 2015.

Berta, M., Bellomo, L., Griffa, A., Magaldi, M.G., Molcard, A., Mantovani, C., Gasparini, G.P., Marmain, J., Vetrano, A., Béguery, L. and Borghini, M.: Wind-induced variability in the Northern Current (northwestern Mediterranean Sea) as depicted by a multi-platform observing system. Ocean Sci., 14, 689-710, https://doi.org/10.5194/os-14-689-2018, 2018.

Buckley, M.P. and Veron, F.: The turbulent airflow over wind generated surface waves, Eur. J. Mech. B. Fluids, 73, 132-143, https://doi.org/10.1016/j.euromechflu.2018.04.003, 2019.

Chang, Y., Hammond, D., Haza, A.C., Hogan, P., Huntley, H.S., Kirwan Jr, A.D., Lipphardt Jr, B.L., Taillandier, V., Griffa, A. and Özgökmen, T.M.: Enhanced estimation of sonobuoy trajectories by velocity reconstruction with near-surface drifters, Ocean Modell., 36, 179-197, https://doi.org/10.1016/j.ocemod.2010.11.002, 2011.

Chassignet, E.P., Smith, L.T., Halliwell, G.R. and Bleck, R.: North Atlantic simulations with the Hybrid Coordinate Ocean Model (HYCOM): Impact of the vertical coordinate choice, reference pressure, and thermobaricity, J. Phys. Oceanogr., 33, 2504-2526, 2003.

Chassignet, E.P., Hurlburt, H.E., Smedstad, O.M., Halliwell, G.R., Hogan, P.J., Wallcraft, A.J., Baraille, R. and Bleck, R.: The HYCOM (hybrid coordinate ocean model) data assimilative system, J. Mar. Syst., 65, 60-83, https://doi.org/10.1016/j.jmarsys.2005.09.016, 2007.

Chen, S.S., Zhao, W., Donelan, M.A. and Tolman, H.L.: Directional wind–wave coupling in fully coupled atmosphere–wave–ocean models: Results from CBLAST-Hurricane, J. Atmos. Sci., 70, 3198-3215, https://doi.org/10.1175/JAS-D-12-0157.1, 2013.

Chen, S.S. and Curcic, M.: Ocean surface waves in Hurricane Ike (2008) and Superstorm Sandy (2012): Coupled model predictions and observations, Ocean Modell., 103, 161-176, https://doi.org/10.1016/j.ocemod.2015.08.005, 2016.

Cole, R., & Symonds, D.: A 25 year collaboration using ADCPs. In 2015 IEEE/OES 11th Current, Waves and Turbulence Measurement Workshop, St. Petersburg, FL, USA, March 2015, 1–10, 2015.

Curcic, M., Chen, S.S. and Özgökmen, T.M.: Hurricane-induced ocean waves and stokes drift and their impacts on surface transport and dispersion in the Gulf of Mexico, Geophys. Res. Lett., 43, 2773-2781, http://doi.org/10.1002/2015GL067619, 2016.

Davis, R.E.: Drifter observations of coastal surface currents during CODE: The method and descriptive view, J. Geophys. Res. C: Oceans, 90, 4741-4755, 1985

Donelan, M.A., Curcic, M., Chen, S.S. and Magnusson, A.K.: Modeling waves and wind stress, J. Geophys. Res. C: Oceans, 117, http://doi.org/10.1029/2011JC007787, 2012.

Ekman, V.W.: On the influence of the Earth's rotation on ocean-currents, Arkiv for Matematik, Astronomi, och Fysik, 2,1-52, 1905.

Gonçalves, R.C., Iskandarani, M., Özgökmen, T. and Thacker, W.C.: Reconstruction of submesoscale velocity field from surface drifters. J. Phys. Oceanogr., in press, http://doi.org/10.1175/JPO-D-18-0025.1, 2019.

5   Haza, A.C., D'Asaro, E., Chang, H., Chen, S., Curcic, M., Guigand, C., Huntley, H.S., Jacobs, G., Novelli, G., Özgökmen, T.M. and Poje, A.C.: Drogue-loss detection for surface drifters during the Lagrangian submesoscale experiment (LASER), J. Atmos. Ocean. Tech., 35, 705-725, http://doi.org/10.1175/JTECH-D-17-0143.1, 2018.

Hill, C., DeLuca, C., Suarez, M. and Da Silva, A.: The architecture of the earth system modeling framework, Comput. Sci. Eng., 6,18-28, https://doi.org/10.1109/MCISE.2004.1255817, 2004.

10   Isobe, A., Kubo, K., Tamura, Y., Nakashima, E. and Fujii, N.: Selective transport of microplastics and mesoplastics by drifting in coastal waters, Mar. pollut. Bull., 89, 324-330, https://doi.org/10.1016/j.marpolbul.2014.09.041, 2014.

Kim, S.Y., Cornuelle, B.D. and Terrill, E.J.: Decomposing observations of high-frequency radar-derived surface currents by their forcing mechanisms: Locally wind-driven surface currents, J. Geophys. Res. C: Oceans, 115, C12046 https://doi.org/10.1029/2010JC006223, 2010.

15   Laxague, N.J., Özgökmen, T.M., Haus, B.K., Novelli, G., Shcherbina, A., Sutherland, P., Guigand, C.M., Lund, B., Mehta, S., Alday, M. and Molemaker, J.: Observations of Near-Surface Current Shear Help Describe Oceanic Oil and Plastic Transport, Geophys. Res. Lett., 45, 245-249, https://doi.org/10.1002/2017GL075891, 2018.

Le Hénaff, M., Kourafalou, V.H., Paris, C.B., Helgers, J., Aman, Z.M., Hogan, P.J. and Srinivasan, A.: Surface evolution of the Deepwater Horizon oil spill patch: combined effects of circulation and wind-induced drift, Environ. Sci. Technol.,

20   46, 7267-7273, https://doi.org/10.1021/es301570w, 2012.

Lumpkin, R., and Pazos, M.: Measuring surface currents with Surface Velocity Program drifters: the instrument, its data, and some recent results, In: Lagrangian Analysis and Prediction of Coastal and Ocean Dynamics, edited by: Griffa, A, Kirwan, A. D., Mariano, A., Özgökmen, T. M., and Rossby, T. Cambridge University Press, Cambridge, 39–67, 2007.

Lumpkin, R., Özgökmen, T. and Centurioni, L.: Advances in the application of surface drifters, Annual Review of Marine

25   Science, 9, 59-81, https://doi.org/10.1146/annurev-marine-010816-060641, 2017.

Novelli, G., Guigand, C.M., Cousin, C., Ryan, E.H., Laxague, N.J., Dai, H., Haus, B.K. and Özgökmen, T.M.: A biodegradable surface drifter for ocean sampling on a massive scale, J. of Atmos. Ocean. Tech. 34, 2509-2532, https://doi.org/10.1175/JTECH-D-17-0055.1, 2017.

Ohlmann, J.C. and Niiler, P.P.: Circulation over the continental shelf in the northern Gulf of Mexico, Prog. Oceanogr., 64,

30   45-81, https://doi.org/10.1016/j.pocean.2005.02.001, 2005.

Özgökmen, T.M., Chassignet, E.P., Dawson, C.N., Dukhovskoy, D., Jacobs, G., Ledwell, J., Garcia-Pineda, O., MacDonald, I.R., Morey, S.L., Olascoaga, M.J. and Poje, A.C..: Over what area did the oil and gas spread during the 2010 Deepwater Horizon oil spill?, Oceanography, 29, 96-107, http://dx.doi.org/10.5670/oceanog.2016.74, 2016.

Phillips, O. M.: Dynamics of the Upper Ocean. Cambridge University Press, Cambridge. 1977.

Pollard, R.T.: On the generation by winds of inertial waves in the ocean, Deep Sea Research and Oceanographic Abstracts, 17, 795-812, https://doi.org/10.1016/0011-7471(70)90042-2, 1970.

Pollard, R.T. and Millard Jr, R.C.: Comparison between observed and simulated wind-generated inertial oscillations, Deep Sea Research and Oceanographic Abstracts, 17, 813-821, https://doi.org/10.1016/0011-7471(70)90043-4 ,1970.

5   Poulain, P.M., Gerin, R., Mauri, E. and Pennel, R.: Wind effects on drogued and undrogued drifters in the Eastern Mediterranean, J.Atmos. Ocean. Techn., 26, 1144-1156, https://doi.org/10.1175/2008JTECHO618.1, 2009.

Rascle, N., Ardhuin, F. and Terray, E.A.: Drift and mixing under the ocean surface: A coherent one-dimensional description with application to unstratified conditions, J. Geophys. Res. C: Oceans, 111, C03016, https://doi.org/10.1029/2005JC003004, 2006.

10 Röhrs, J., Sperrevik, A.K., Christensen, K.H., Broström, G. and Breivik, Ø.: Comparison of HF radar measurements with Eulerian and Lagrangian surface currents. Ocean Dyn., 65, 679-690, https://doi.org/10.1007/s10236-015-0828-8, 2015.

Sentchev, A., Forget, P. and Fraunié, P.: Surface current dynamics under sea breeze conditions observed by simultaneous HF radar, ADCP and drifter measurements, Ocean Dyn., 67, 499-512, https://doi.org/10.1007/s10236-017-1035-6, 2017.

Skamarock, W.C., Klemp, J.B., Dudhia, J., Gill, D.O., Barker, D.M., Duda, M.G., Huang, X.Y., Wang, W. and Powers, J.G.:
15   A description of the advanced research WRF version 3, NCAR Technical Note NCAR/TN-475+STR, National Center for Atmospheric Research, http://dx.doi.org/10.5065/D68S4MVH, 2008.

Stewart, R.H. and Joy, J.W.: HF radio measurements of surface currents, Deep Sea Research and Oceanographic Abstracts, 21, 1039-1049, https://doi.org/10.1016/0011-7471(74)90066-7, 1974.

Stokes, G. G.: On the theory of oscillatory waves, Transactions of the Cambridge Philosophical Society, 8, 441-473, 1847.

20 Taillandier, V., Griffa, A. and Molcard, A.: A variational approach for the reconstruction of regional scale Eulerian velocity fields from Lagrangian data, Ocean Modell., 13, 1-24, https://doi.org/10.1016/j.ocemod.2005.09.002, 2006.

Wallcraft, A.J., Metzger, E.J. and Carroll, S.N.: Software design description for the Hybrid Coordinate Ocean Model (HYCOM) version 2.2, Naval Research Laboratory Tech. Rep. NRL/MR/7320-09-9166, NRL, 2009.

Wu, J.: Sea-surface drift currents induced by wind and waves, J. Phys. Oceanogr., 13, 1441-145,
25   https://doi.org/10.1175/1520-0485(1983)013<1441:SSDCIB>2.0.CO;2, 1983.

Literature	Instrument Used	Measurement Depth	Wind Magnitude	Avg. Velocity of Wind-Driven Current (% of Wind)	Avg. Deflection Angle to the Right of Wind
Ardhuin et al. 2009	HF radar	0-1 m	1-19 m s^{-1}	0.4 – 0.8 %	45° - 70°
Kim et al. 2010	HF radar	0-1 m	1-5 m s^{-1}	2 – 5 %	50° - 90°
Berta et al. 2018	HF radar	0-0.75 m	10-20 m s^{-1}	2 %	25° - 30°
Sentchev et al. 2017	ADCP	0.5-0.75 m	1-6 m s^{-1}	2 – 4 %	12° - 25°
Poulain et al. 2009	Undrogued SVP drifter CODE drifter	0-2.5 m 0-1 m	0-15 m s^{-1}	2 % 1 %	17° - 20° 28° - 30°
Current Work	CARTHE Undrogued CARTHE Drogued	0-0.05 m 0-0.60 m	11-20 m s^{-1}	3.6-6 % 2.3-4.1 %	5° - 55° 30° - 85°

Table 1: Review of literature on wind-driven surface currents using real ocean, observational data.
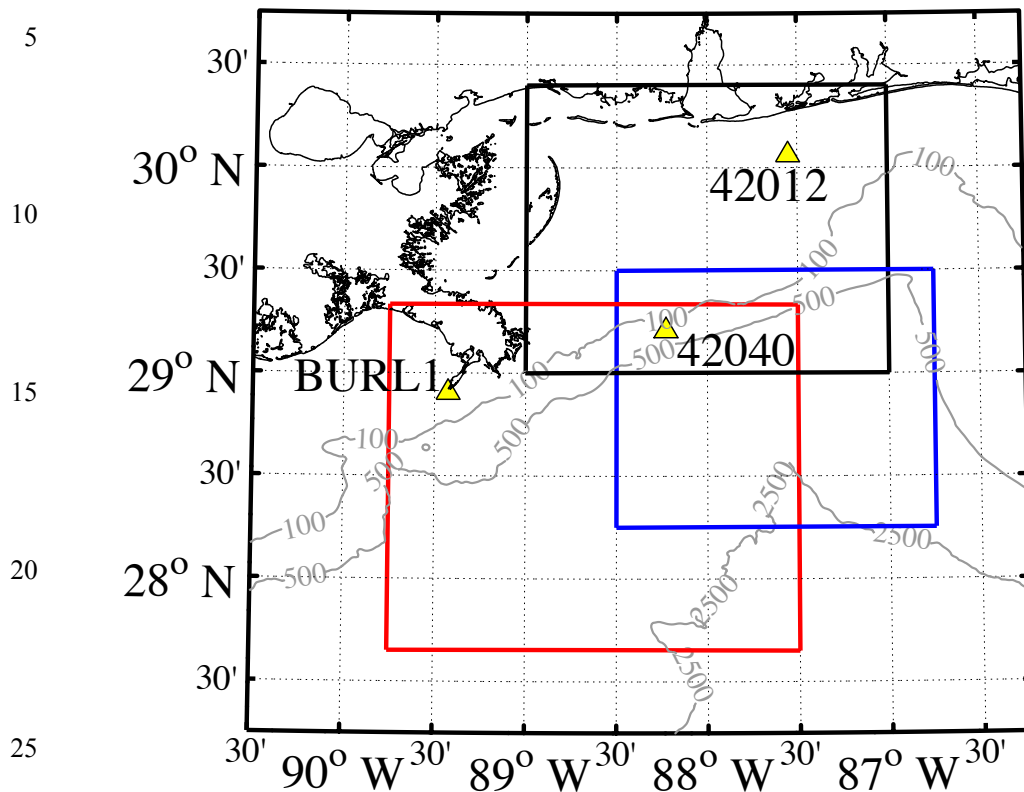
Figure 1: Research area in the Northern Gulf of Mexico, ESE of the Mississippi River delta. NDBC buoy locations used for validation of UWIN-CM U10 wind data are shown by yellow triangles. Domains corresponding to each high event analyzed are shown in the red (February 24th), blue (January 22nd), and black (March 20th) boxes. Grey contours show the bathymetry at 100, 500 and 2500 meters.
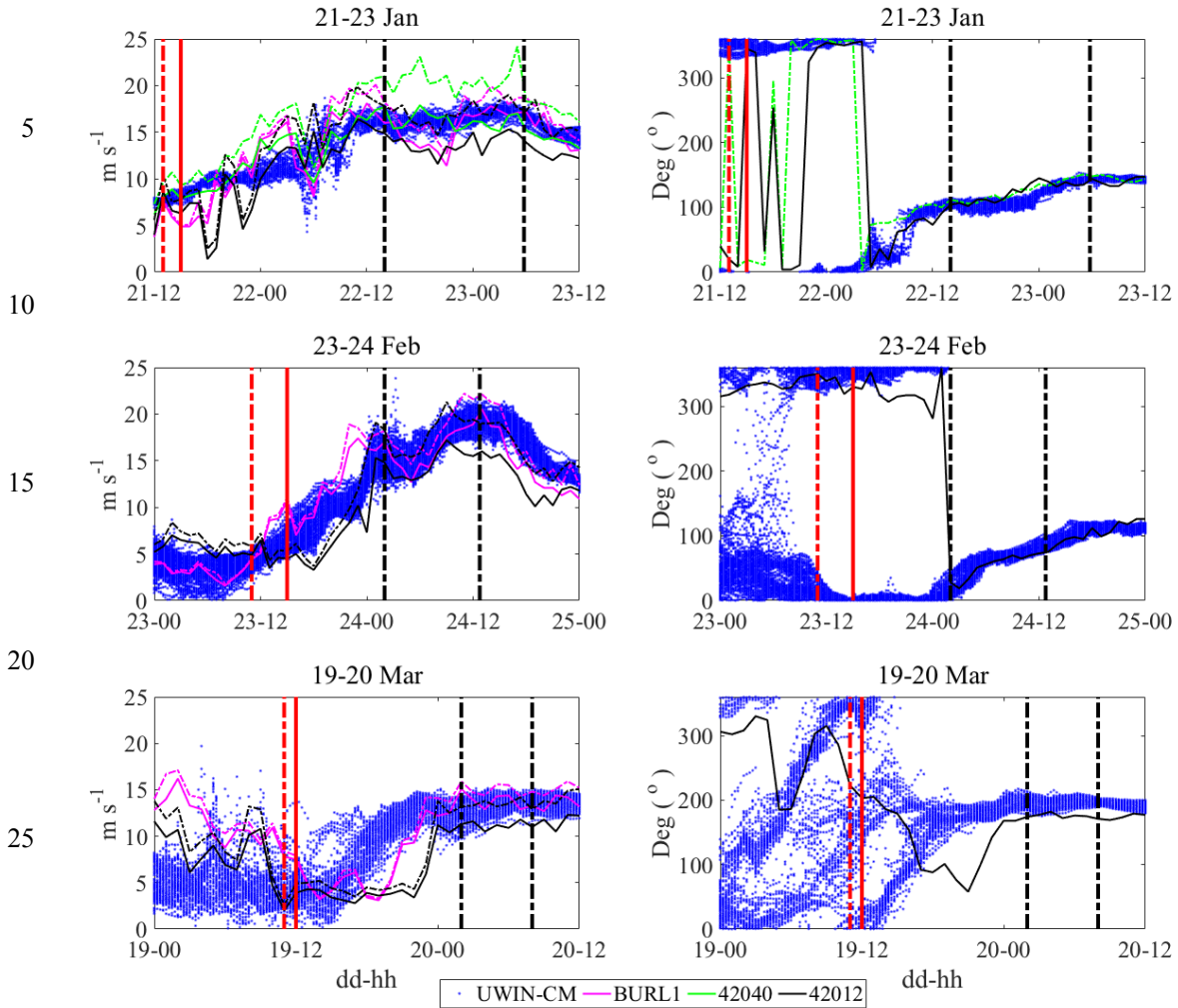
Figure 2: Wind velocity magnitudes (left) and directions (right) during the hours preceding, and including, each high wind event. Black dashed vertical lines show the beginning and end of the high wind analysis periods. Red dashed(solid) red lines indicate beginning of the hour over which the pre-existing regional circulation was estimated with undrogued(drogued) drifters. U10 wind data from the UWIN-CM are plotted at the nearest point to every drifter location. Wind observations from NDBC buoys BURL1, 42040, an 42012 are plotted as well. Solid lines show sustained winds, while dashed lines show wind gusts. All wind directions are plotted as the direction in which the wind is traveling. Buoy 42040 was only operational during the first wind event and BURL1 did not record any wind direction data during the experiment.
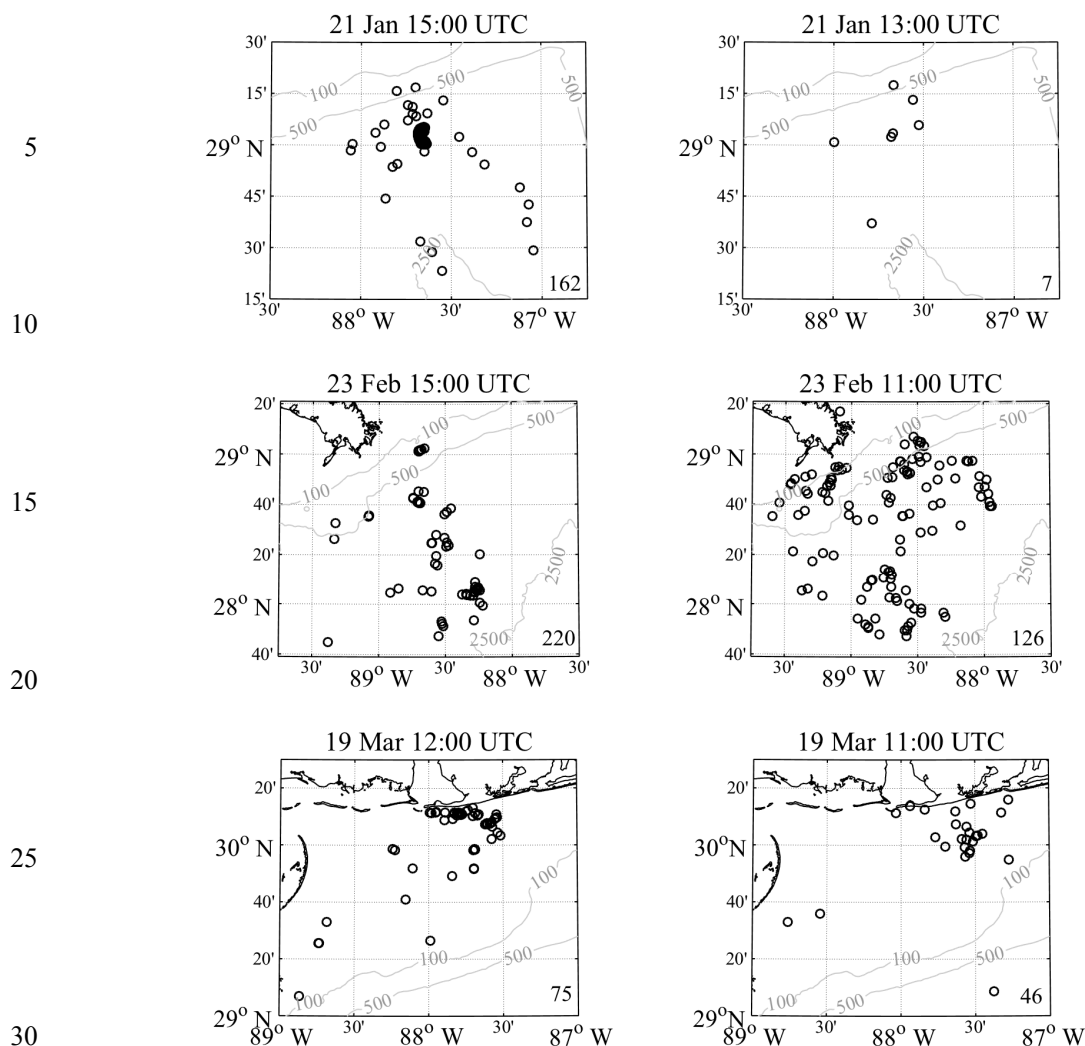
Figure 3: Drogued (left) and undrogued (right) drifters used to create Eulerian velocity fields of the pre-wind event regional circulation estimates using the LAgrangian Variational Analysis (LAVA). Raw drifter locations are plotted at the end of the hour over which the velocity fields are created. Numbers in bottom right corner of plots display the number of drifters used for each velocity field construction. Panels correspond to sub-domains shown in Figure 1.
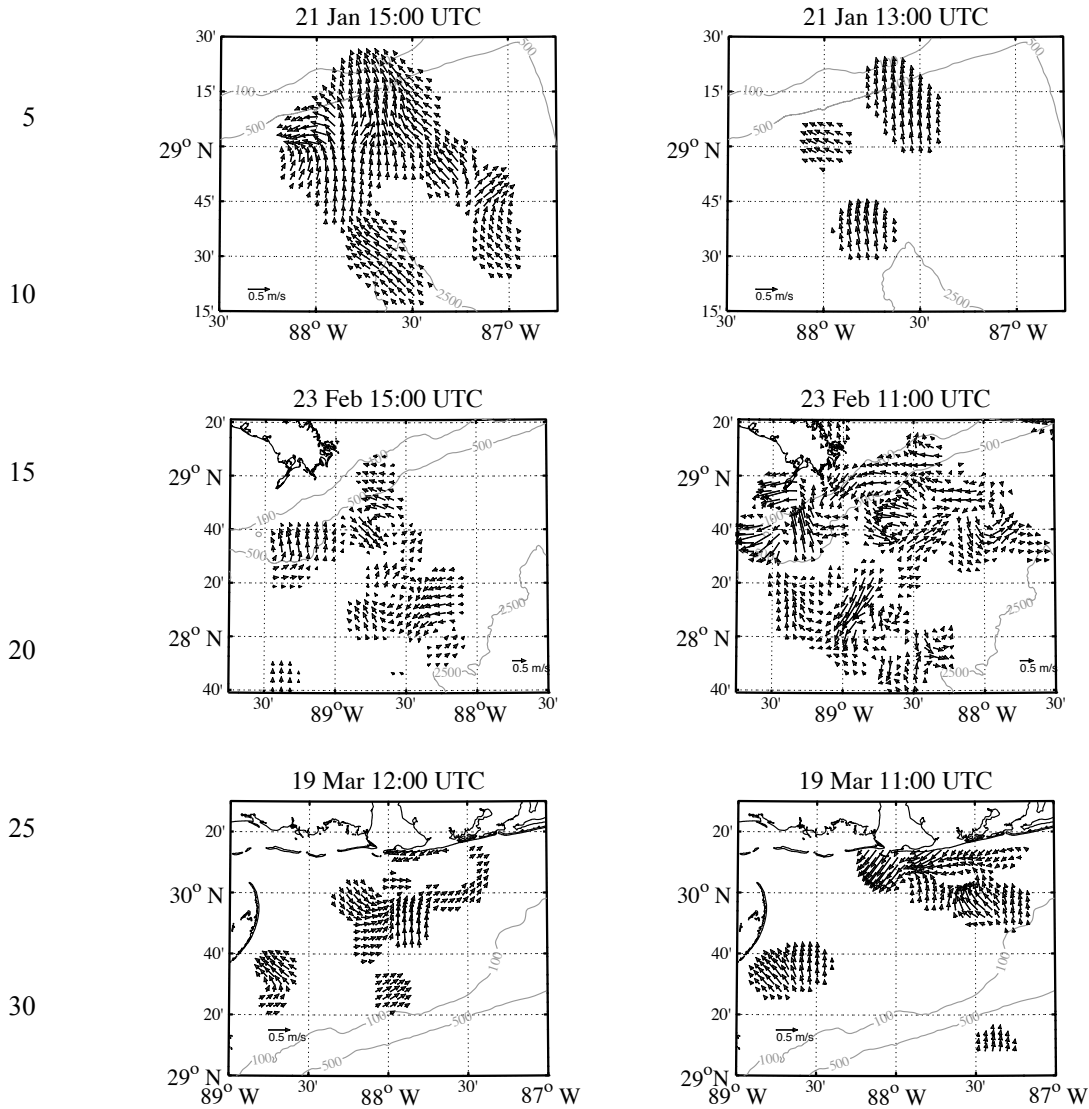
Figure 4: Eulerian velocity fields of the regional circulation that preceded each high wind event, created using LAVA for drogued (left) and undrogued (right) drifters in the area. Titles of each plot list the beginning of each hour over which the velocity field was created from drifter trajectories. In each velocity field, every third vector is plotted for visibility.
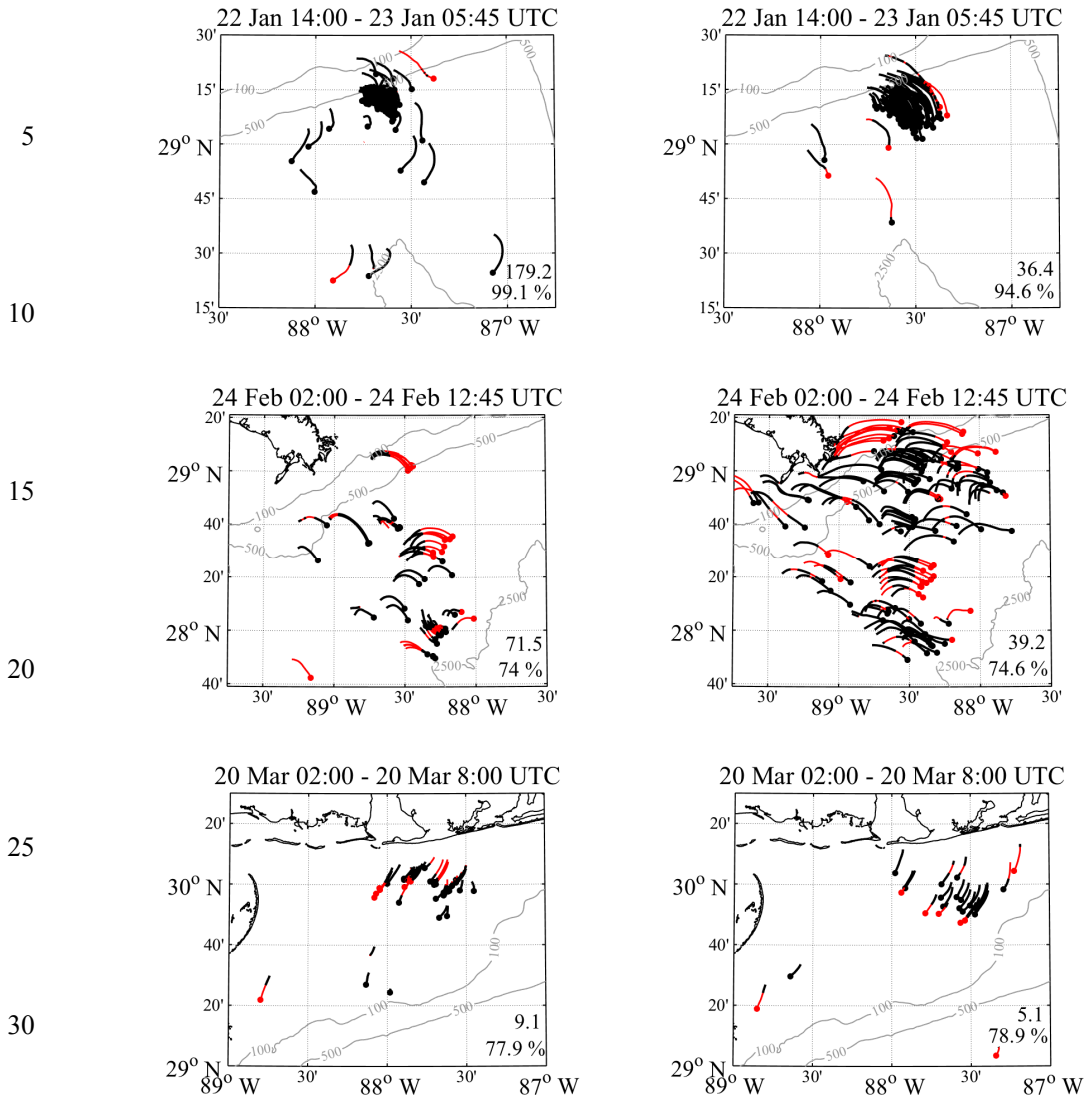
Figure 5: Drogued (left) and undrogued (right) drifter trajectories during the hours of analysis for each high wind event. Time periods over which the total velocity deconstructions were calculated are shown in each title. Portions of the trajectories shown in black (red) depict segments which overlap (do not overlap) spatially with each respective Eulerian velocity field in Fig 4. (Top) the total number of retained trajectory data points, defined as number of drifter days given 15-minute time steps, and (bottom) the percentage of coverage between trajectories and each respective Eulerian velocity field in Fig.4 are listed within each plot. Trajectories missing head markers are a result of either drogue loss or lost GPS transmission during the experiment.
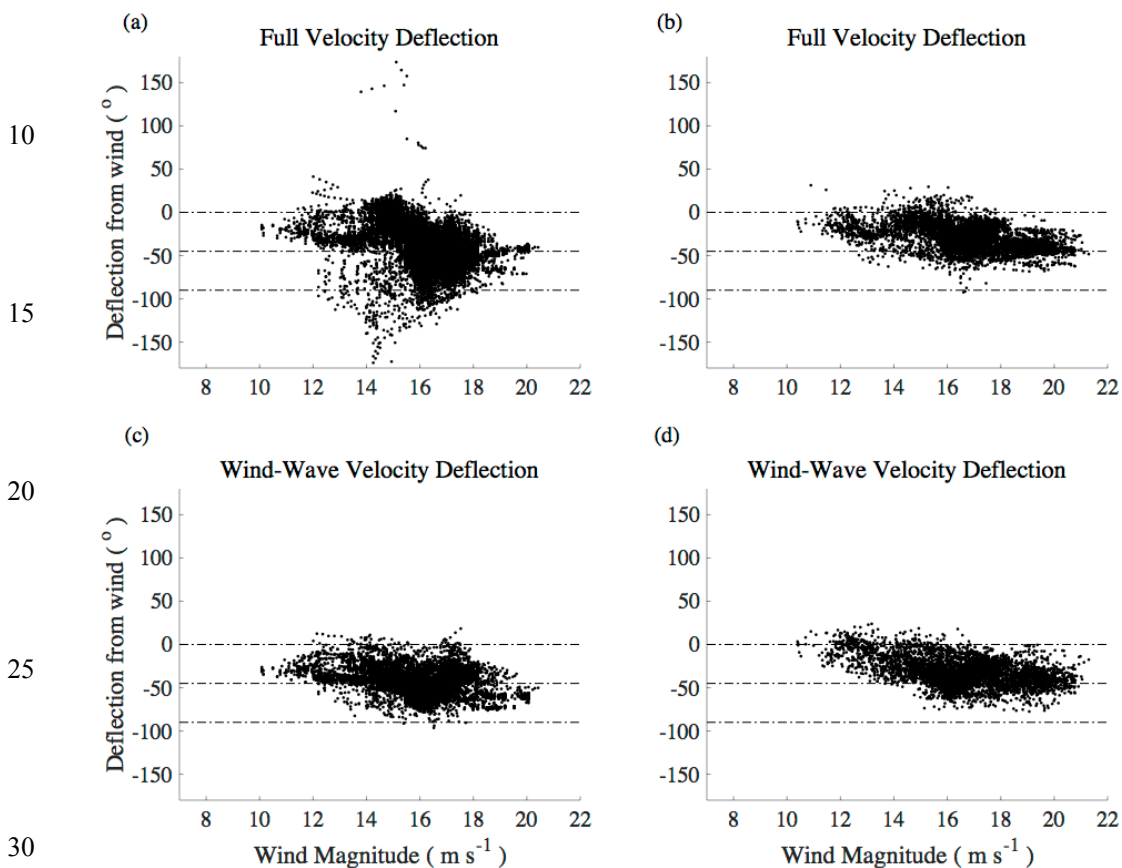
Figure 6: Scatter plots of deflection angles of drogued (a,c) and undrogued (b,d) drifter velocities before (a,b) and after (c,d)
35 **subtracting the pre-existing regional circulation velocity fields during the high wind periods analyzed. Data points that do not have**
both individual drifter velocity measurements and coinciding data in the Eulerian velocity fields of the pre-existing circulation
during the high wind event are not included. Deflection angles are plotted against the U10 wind magnitude from the UWIN-CM
model at the nearest point to the drifter locations in the domain.
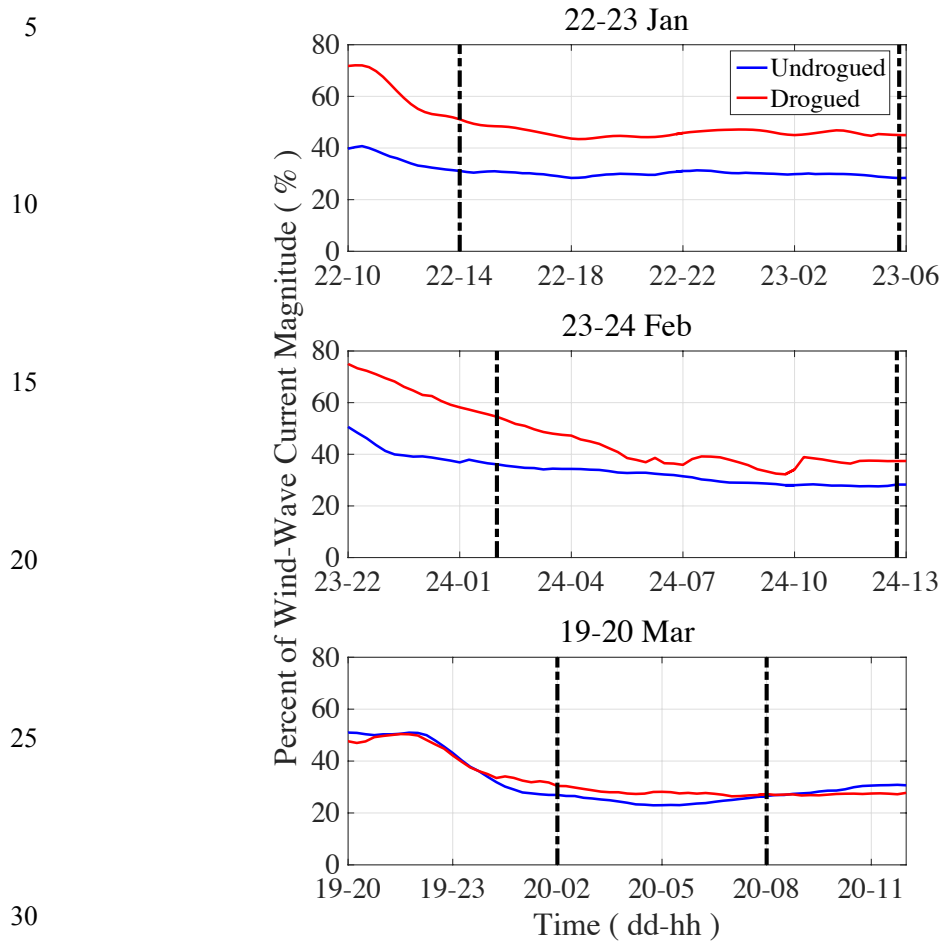
Figure 7: Average of the Eulerian velocity field estimates of the pre-wind regional circulation plotted as a percentage in time of the average combined wind- and wave-driven flow for drogued and undrogued drifters. Vertical dashed lines depict the analysis period for the total velocity deconstruction.
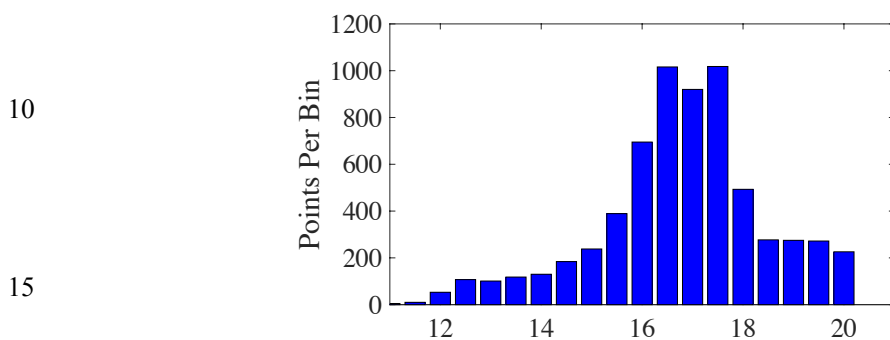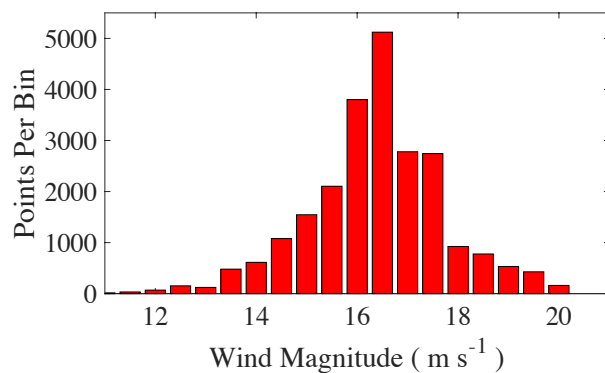
Figure 8: Number of undrogued (top) and drogued (bottom) drifter positions where the velocity deconstruction was performed, binned by wind velocity magnitude on 0.5 m s⁻¹ intervals. Point velocity measurements calculated from drifter trajectories that do not coincide spatially with available data in the pre-existing circulation velocity fields are not included.

35
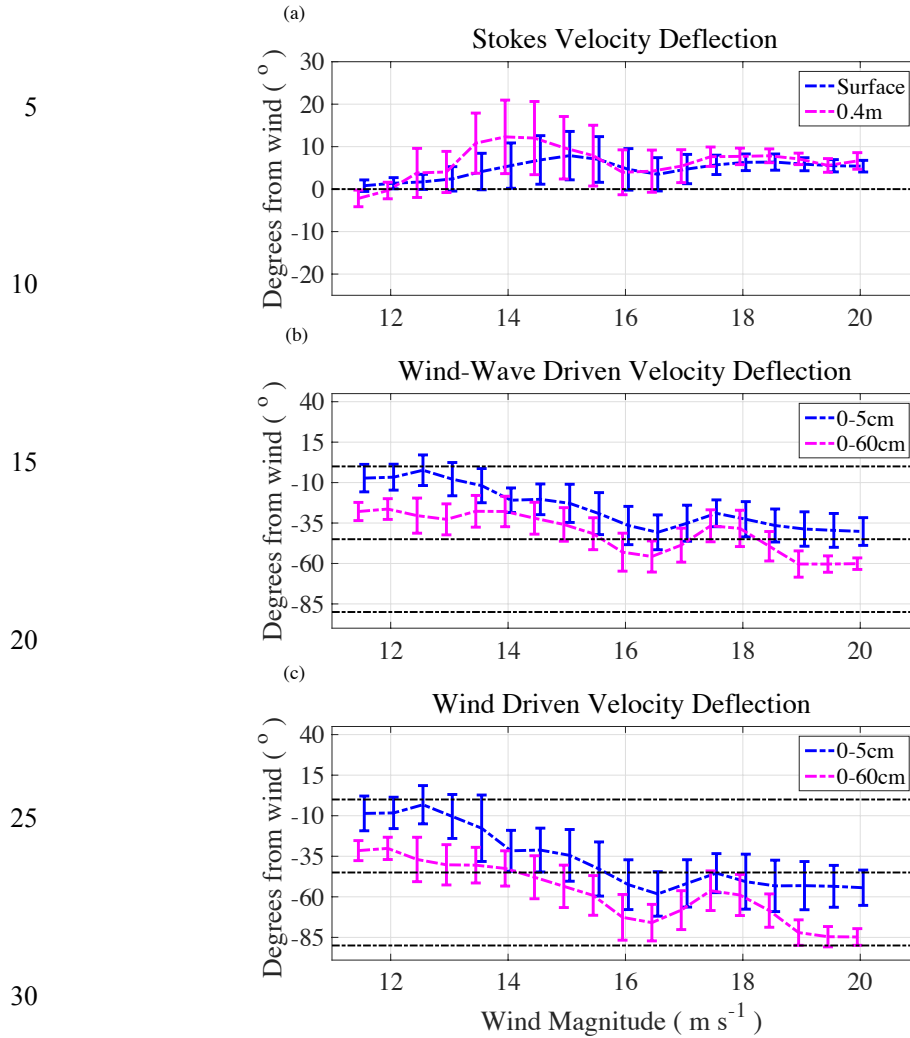
Figure 9: Average deflection angles at drifter locations during periods of high wind binned by UWIN-CM wind magnitudes on 0.5 m s⁻¹ intervals. Horizontal dotted lines denote 0°, 45°, and 90° to the right of the wind. (a) UWIN-CM Stokes drift velocity direction at the surface (0 m) and at 0.4 m depth. (b) Velocity direction of drogued and undrogued drifters after the subtraction of the pre-existing circulation estimate. (c) Velocity direction of the purely wind-driven component of the drifter velocities. All error bars show +/- one standard deviation within each bin. Data in wind bins lower than 11.5 m s⁻¹ were omitted due to lack of data points and large standard deviations.
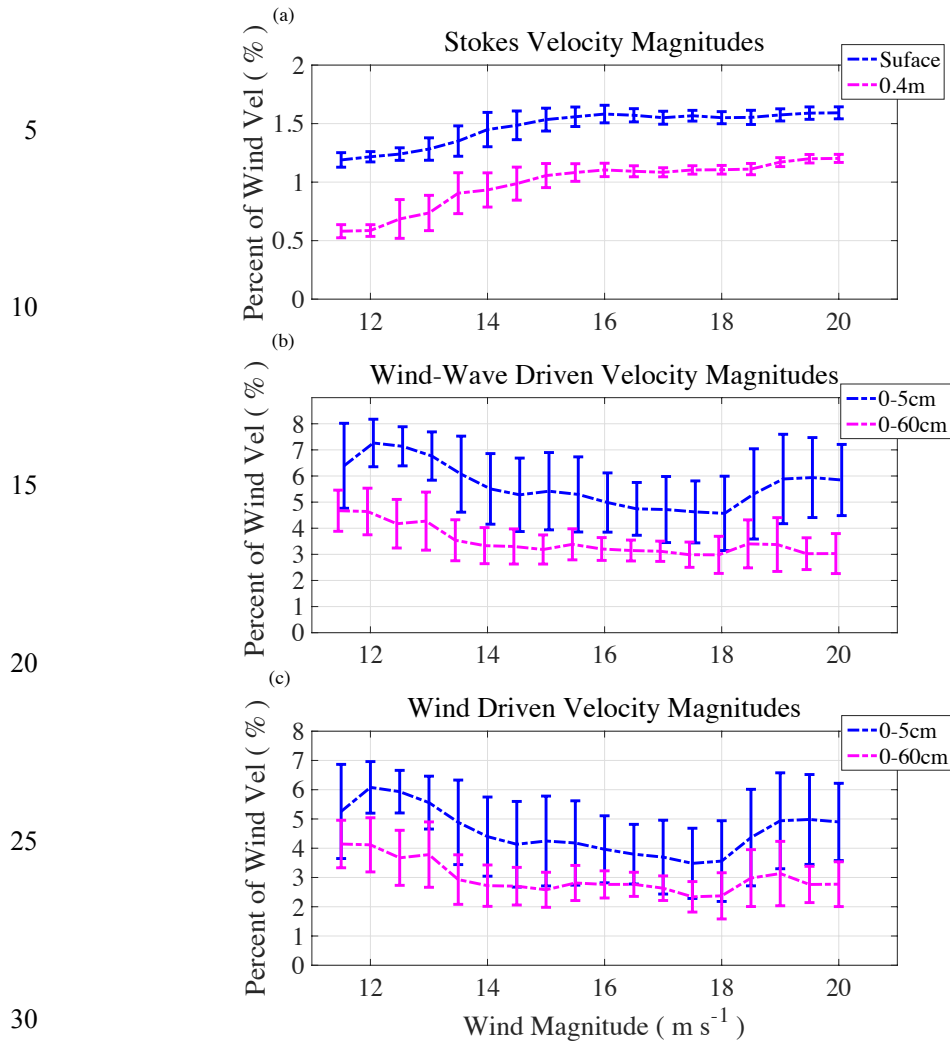
Figure 10: Average velocity magnitudes at drifter locations during periods of high wind binned by UWIN-CM wind magnitude on 0.5 m s^{-1} intervals. (a) UWIN-CM Stokes drift velocity magnitude at the surface (0 m) and at 0.4 m depth. (b) Velocity magnitude of drogued and undrogued drifters after the subtraction of the pre-existing circulation estimate. (c) Velocity magnitude of the purely wind-driven component of the drifter velocities. All error bars show +/- one standard deviation within each bin. Data bins omitted in Figure 9 are also excluded.